Available online at www.sciencedirect.com

ScienceDirect

materialstoday: PROCEEDINGS

Materials Today: Proceedings 3 (2016) 867 – 874

12th International Conference on Nanosciences & Nanotechnologies & 8th International Symposium on Flexible Organic Electronics

# Exploring and evaluating micro-environment and nanoparticle dielectrophoretic-induced interactions with image analysis methods☆

David J. Bakewell[1]*, Joe Bailey[2,3], David Holmes[2,4]

[1]*Department of Electrical Engineering and Electronics, University of Liverpool, Liverpool, L69 3GJ, UK*
[2]*London Centre for Nanotechnology, University College London, London, WC1H 0AH, UK*
[3]*CoMPLEX: Centre for Mathematics, Physics, Life Science and Experimental Biology, University College London, London, WC1E 6BT, UK*
[4]*Sphere Fluidics Ltd, Babraham Research Campus, Babraham, Cambridge, CB22 3AT, UK*

**Abstract**

Nanoparticle interactions with micron-scale environments can be induced using dielectrophoresis (DEP). A new DEP signaling and additive noise model is developed from first principles. It is applied to fluorescence microscope CCD video images of fluorescently labeled, 200 nm diameter, latex nanospheres moved by pulsed, positive DEP (pDEP) onto 5 micron planar castellated electrode edges. The model increases the signal-to-noise ratio (SNR) for the time dependent spatial mean of the video frame fluorescence intensity and thereby enables correlation with the spatial standard deviation (std) statistic. Deterministic pDEP-induced collections are approximately linearly correlated, whereas thermally-driven, random, nanoparticle movements are nonlinearly correlated.


Selection and peer-review under responsibility of the Conference Committee Members of NANOTEXNOLOGY2015
(12th International Conference on Nanosciences & Nanotechnologies & 8th International Symposium on Flexible Organic Electronics)

*Keywords:* dielectrophoresis; electrokinetics; nanoparticle; image analysis; signal-to-noise ratio



* Corresponding author. Tel.+44-780-799-5656.
*E-mail address:*davidjgbakewell@gmail.com

2214-7853 
Selection and peer-review under responsibility of the Conference Committee Members of NANOTEXNOLOGY2015 (12th International Conference on Nanosciences & Nanotechnologies & 8th International Symposium on Flexible Organic Electronics)
doi:10.1016/j.matpr.2016.02.020

## 1. Introduction

Real-time probing and microscopic observation of nanoparticle motion, within spatially-structured micron-scale environments, can be induced using an electrokinetic method known as dielectrophoresis (DEP) [1]. DEP is the translational movement of an electrically polarizable body, suspended in a suitable medium, by the action of an externally applied non-uniform electric field [2]. The body can be electrically charged or neutral, as the net force on the body arises from a vector sum of induced dipoles locally interacting with the applied inhomogeneous electric field. DEP is typically implemented by applying a low voltage radio frequency (RF) electrical signal to microfabricated electrodes immersed in an electrolyte of low conductivity. It is a useful and popular electrokinetic technique that can be conveniently integrated into lab-on-chip (LOC) platforms [3-5].

The small-time averaged DEP force can be written as,

$$\vec{F}_{DEP}(\underline{x},t_s) = 2\pi r^3 \varepsilon_m \,\mathrm{Re}\{f_{CM}[\omega(t_s)]\}\vec{\nabla}|\vec{E}(\underline{x},t_s)|^2 \qquad (1).$$

where $\underline{x}$ is the spatial position, $r$ is the spherical nanoparticle radius, $\varepsilon_m$ is the medium permittivity, $\vec{\nabla}$ is the gradient operator, $\rightarrow$ denotes vector quantity, $|\vec{E}|$ is the electric field magnitude (rms), $\mathrm{Re}\{f_{CM}[\omega(t)]\}$ is the real part of the Clausius-Mossotti (CM) function with angular frequency, $\omega(t) = 2\pi f(t)$ and $f$ is the RF [3, 5]. In (1), it is understood $|\vec{E}|$ and $f$ are mostly constant and can be *switched* at selected times, $t_s$, and $\mathrm{Re}\{f_{CM}(\omega)\}$ is dependent on the material properties (permittivity and conductivity) of both the particle and surrounding electrolyte medium. Positive DEP (pDEP) occurs when particles are attracted to regions where $\vec{\nabla}|\vec{E}(\underline{x})|^2$ is high and conversely negative DEP (nDEP) occurs when particles are repelled from these regions.

The dependence of the DEP force on the geometric and material properties of the nanoparticle, electrolyte medium, micro-environment encasing the nanoparticle suspension and applied electric field, shown in (1), has been the basis for much research on DEP. There have many studies involving the separation of particles according to the differences in frequency dependent dielectric nanoparticle properties, often including differences in size, and using either batch processing or flow-through micro-fluidic platforms. Considerable research on electrode materials and design has resulted in advanced functionality and versatility. There have also been developments for measuring the motion of nanoparticles, and related biological entities, in-part to determine unknown dielectric parameters, e.g. measuring initial collection rates of cells, viruses, DNA, RNA, etc., as cited in [2, 5-10] and references therein.

In comparison, there have been relatively few systematic studies on using nanoparticle movement, imaged microscopically in real-time, that use DEP-induced nanoparticle interactions to make inferences about micro-environment properties. Applications include, for example, the detection of defects of microfabricated electrodes, not visually obvious, that can arise during clean-room lift-off and other processes. Nanoparticles in fluid medium exhibit deterministic motion, induced by DEP or other forces (e.g. fluid motion, sedimentation), and random Brownian motion, arising from the incessant collisions with electrolyte molecules. In addition, there are many other sources of temporal fluctuation in a DEP signaling and image quantification system, e.g. camera noise, fluctuations in light, etc. Hence, the strength of inference depends on obtaining the best possible measurement of deterministic motion compared with random noise. A key performance parameter, therefore, is the signal-to-noise ratio (SNR). To achieve traditional applications of nanoparticle DEP and for novel probing of the micro-environment, our paper advances previous work [1, 6, 11] by developing new methods for improving the SNR of a DEP signaling and image quantification system.

## 2. Background

The DEP signaling and image quantification system under consideration is shown in Fig. 1(a). The scheme shows a computer controlled RF electric signal generator that supplies planar electrodes with voltage to induce DEP motion and an inverted fluorescence microscope for nanoparticle observation and camera recording. As shown in Fig. 1(b)(i) during DEP off, nanoparticles diffuse randomly so that their distribution within a confined chamber volume becomes uniformly distributed. When DEP is switched on the pDEP forces result in nanoparticles moving towards the electrode tips, as shown in Fig. 1(b)(ii) and is called the *collection phase*. Switching DEP off allows nanoparticles to diffuse and be 'released' from the electrode tips and is called the *release phase*. A single cycle, or *pulse*, typically comprises a collection (pDEP on) and release phase (pDEP off). To reduce the amount of experimental uncertainty, two cycles or a *dual-cycle* is used. Referring to Fig. 1(c), the first cycle collection phase uses a constant frequency that acts as a *control* and the second cycle collection phase uses a *probe* frequency of interest chosen by the investigator. Conventional pDEP nanoparticle movement, e.g. initial collection rates, is often quantified by measuring the optical intensity (e.g. fluorescence) frame-by-frame. Quantification of the two dimensional (2D) spatial intensity for each frame can yield noisy and unsatisfactory collection time profiles, so that filtering methods are needed to improve the SNR, as indicated in the figure. In the following section, measures and tools from the two filtering methods, geometric- and statistic-based [1, 11], are used for new purposes to further enhance the SNR of the system.

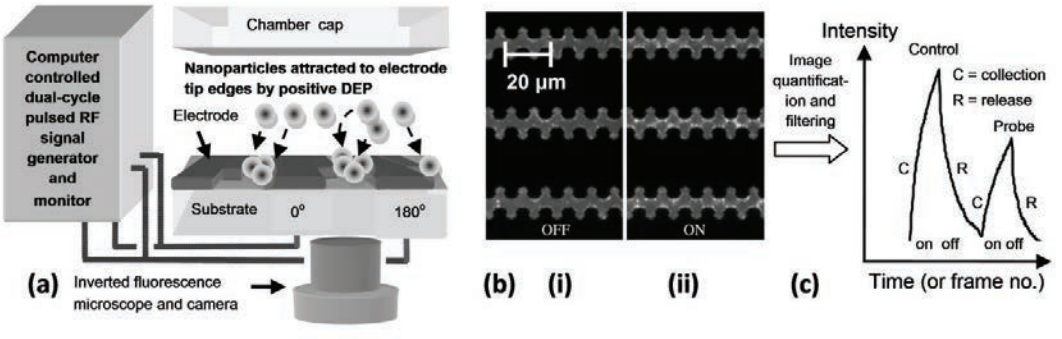


Fig. 1. (a) Schematic of pulsed pDEP experimental arrangement. (b) Typical partial-frame images of fluorescent nanoparticle suspension with pDEP (i) *off* and (ii) *on.* The dark regions are the castellated electrodes and the nanoparticles are represented by medium-grey to white pixels. During the 'on' state fluorescently labeled nanoparticles (white) collect at the electrode tips as an AC signal is applied. (c) Image quantification and filtering leads to dual-cycle (showing control and probe cycles, collection and release phases for each cycle).

## 3. Materials and methods

### *3.1. Probabilistic fluorescence intensity*

The intensity detected on the CCD camera can be written as random variable (RV), $I_g$, where subscript '$g$' denotes grayscale (0 - 255), that has two statistically independent components,

$$I_g = I_\lambda + I_\delta \tag{2}.$$

The first component is the fluorescence *light* intensity, $I_\lambda$, and the second is the *dark* noise associated solely with CCD detection, $I_\delta$, that occurs in the absence of light (RV components are denoted by lowercase Greek subscripts).

It is understood that the RVs are dependent on the 2D pixel positions in each video frame and on time, *t*, so that these variables are implicit.

The discrete distribution for each video frame intensity can be expressed in terms of the partitioned probabilities [11, 12] for non-overlapping 2D image areas, or regions,

$$P(I_g = i_g) = P(I_g = i_g \mid \Omega_G)P(\Omega_G) + P(I_g = i_g \mid \Omega_C)P(\Omega_C) + P(I_g = i_g \mid \Omega_{I_E})P(\Omega_{I_E}) \quad (3).$$

In (3), $P(I_g = i_g \mid \Omega_A)$ reads as the probability of RV, $I_g$, being equal to a discrete grayscale value, $i_g$, is conditioned on detection events occurring in a partitioned sample space, or image area, $\Omega_A$, within the entire frame region, $\Omega_F$. Annotated examples of frame intensity images, $I_F(t)$, are shown in Fig. 2(a) and 2(b).

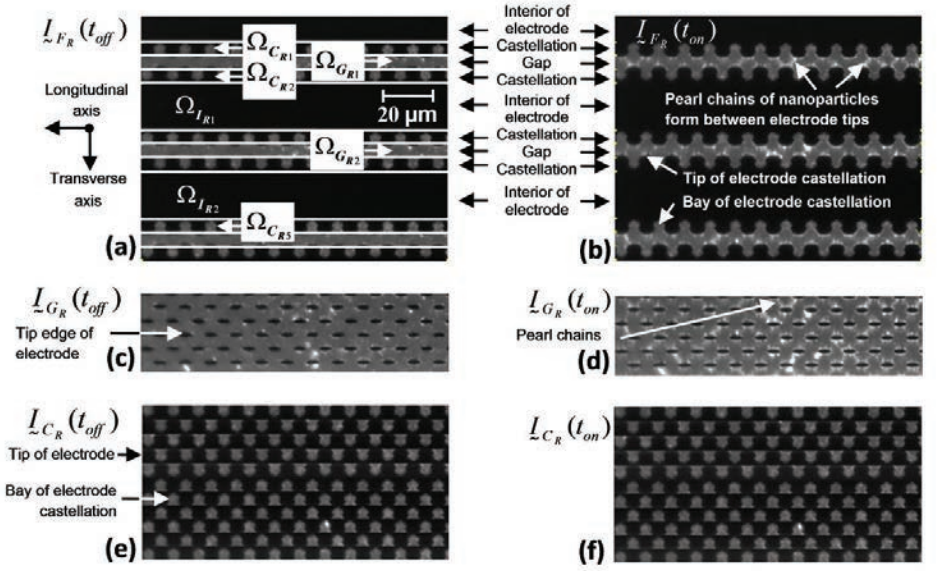


Fig. 2 Typical video images: DEP off ($t$ = 0.3 s) shown in (a), (c) and (e); DEP on ($t$ = 43.0 s) shown in (b), (d) and (f). In (a) video frames are superposed with white boundaries that partition 2D sample space regions, or longitudinal strips, as labeled. Interior of electrode (dark), castellation and inter-electrode gap regions are denoted by subscripts '*I*', '*C*', '*G*', respectively. Sub-subscript '*R*' denotes half-width, half-height (quarter) frame size *representation* for illustration and numbers indicate sub-regions. In (b) planar electrode array features and nanoparticle pearl chain formations are labeled as shown. Composite images, formed by juxtaposing matrix rows, are shown for the gap, (c) and (d), and castellation, (e) and (f), regions (six and eleven strips), respectively. Image intensities shown in (c) to (f) are symbolized in the form $\underset{\sim}{I}_{A_R}(t)$ where ~ denotes 2D matrix image, subscripts denote regions, and '*R*' denotes half-width frame for illustrative *representation*. The images show that the nanoparticles collect (medium grey to white pixels), under the action of pDEP, largely within the gap region, i.e. between the electrode tips and across the transverse inter-electrode gaps. On the other hand, the castellation region appears relatively unchanged. See text for details.

Subscripts '*F*' and '*R*' denote *frame* and *representation* for illustration that is half-width, half-height (quarter size). Each frame matrix is partitioned into strips parallel to the longitudinal axis (rows of column elements), as shown in Fig. 2(a). Sample areas of the gap, $\Omega_G$, castellation, $\Omega_C$, and interior of electrode, $\Omega_{I_E}$, are denoted by subscripts '*G*', '*C*' and '$I_E$', respectively. Juxtapositions of gap and castellation image strips, that constitute the frame partly shown in Fig. 2(a) and (b), for pDEP off and on, are shown in Figs. 2(c) to (f). The non-overlapping sub-regions constitute the areas, $\Omega_{G_R} = \bigcup_{k=1}^{6} \Omega_{G_k}$ and $\Omega_{C_R} = \bigcup_{k=1}^{11} \Omega_{C_k}$, respectively, where $\bigcup$ denotes union and subscript '*R*'

denotes half-frame width *representation* for illustration. The selection of the gap region is shown, in Figs. 2(c) to (f), to include most of the nanoparticles that can be captured by pDEP whereas the castellation region remains unchanged. Juxtapositions of the interior of electrode regions, for conciseness, are not shown. The number of pixels, $n_p$, in a region of interest is the product of the number of rows, $n_{\mathrm{rw}}$, and columns, $n_p = n_{\mathrm{rw}} \times 640$. Symbols and values for the number of pixels constituting the gap, castellation, interior and frame are listed in Table 1 along with the expressions and values for the conditional probabilities, or weight coefficients.

Expressions for the spatial mean and standard deviation (std) for the intensity RV are found from the first and second moments,

$$I_m(t) = \sum_{i_g=0}^{i_{g_x}} i_g^m . P(I_g = i_g) = \frac{1}{n_p} \sum_{k=1}^{n_p} I_g^m(k,t) \tag{4}$$

where $m = 1, 2$. The mean is the first moment, $\mu(t) = E[I_g(t)] = I_1(t)$ where $E[\ ]$ denotes *expected value*. The asymptotically unbiased estimator of the std [12], applicable for large $n_p$ is,

$$\sigma(t) = \sqrt{I_2(t) - I_1^{\,2}(t)} \tag{5}.$$

Table 1. Partitioned video frame image details - all 512 rows entail 640 column pixels

| Region | Number of rows | Number of pixels | | Conditional probabilities | |
|---|---|---|---|---|---|
| | | Symbol | Value | Expression and weight coefficient | Value |
| Gap | 81 | $n_G$ | 51840 | $P(\Omega_G) = n_G / n_F = \gamma$ | 0.158 |
| Castellation | 159 | $n_C$ | 101760 | $P(\Omega_C) = n_C / n_F = \chi$ | 0.311 |
| Interior | 272 | $n_{I_E}$ | 174080 | $P(\Omega_{I_E}) = n_{I_E} / n_F = \iota_\varepsilon$ | 0.531 |
| Frame (total) | 512 | $n_F$ | 327680 | $P(\Omega_F) = 1$ | 1.000 |

### *3.2. Experimental arrangements*

Referring to Fig. 1(a) to (c), an arbitrary function generator (Tektronix AFG 3022B, OR, USA) was used to provide 2 V peak-to-peak, square wave enveloped, sinusoidal signals to the microelectrodes. The duty cycle was 7 s on, 10 s off per cycle, and the control and probe RFs were 700 kHz and 3.0 MHz, respectively. Pulse duration, amplitude and applied frequencies were controlled by custom software written in LabVIEW™ 2011 (National Instruments Corp., Austin, TX, USA). Castellated geometry interdigitated microelectrodes with critical feature sizes of 5 microns were fabricated using standard photolithography and lift-off techniques. A 100 nm thick layer of platinum was lithographically patterned on 500 μm thick Pyrex wafers. Individual devices were cut from the wafer, mounted on Veroboard and wire bonded so as to ensure robust electrical connection to the signal generator. A 3 mm diameter sample reservoir was fabricated in poly-dimethylsiloxane (PDMS). The PDMS and glass chip were exposed to an $O_2$ plasma to facilitate bonding of the PDMS to the glass/platinum substrate. The completed device was then sealed with a cover-slip to prevent sample evaporation.

Ultra-pure water having a resistance of 18.2 MΩcm (Purelab ultra, Elga process water, Buckinghamshire, UK) was used to prepare KCl (Sigma-Aldrich® Inc., ST Louis, MO) electrolyte solutions with conductivity of $2\times10^{-4}$ S/m (Mettler Toledo, InLab® 730, Columbus, OH) at room temperature. Carboxylate modified 200 nm diameter

latex spheres (Invitrogen™ Molecular Probes®, Eugene, OR) with yellow-green fluorescence (505/515 nm wavelength) were washed three times in KCl electrolyte solution ($2\times10^{-4}$ S/m) and suspended in the same medium at a concentration of $5\times10^{10}$ spheres/ml (diluted 1:100 from 2% w/v stock solution). The concentration and monodispersity of the nanospheres was verified using nanoparticle tracking analysis (NanoSight LM10, Wiltshire, UK). The motion of the nanospheres was observed using an inverted microscope (Axiovert 200M, Zeiss, Germany) with epi-fluorescent illumination (HBO100, Zeiss), imaged with a x40 objective and recorded with a digital camera (Thorlabs USB 2.0, Newton, NJ) at 10 frames/s. Referring to Fig. 2(a) to (f), videos were analyzed using software written in Mathematica™ 8 (Wolfram Research, Campaign, IL) and Matlab™ 7.14 (Mathworks Inc., Natick, MA) using methods described in [11]. Nanosphere collections at the high-field gradient areas of the castellated electrodes (i.e. regions where particles collect under the influence of pDEP) were quantified by measuring the fluorescence intensity at the electrode tips.

## 4. Results: theoretical and experimental

Substituting equation (3) into (4) yields the relation for the time dependent spatial mean, or expectation, of the frame intensity,

$$\mu_F(t) = \gamma\,\mu_G(t) + \chi\,\mu_C(t) + \iota_\varepsilon\,\mu_{I_E}(t) \tag{6}$$

where $\mu_G(t)$, $\mu_C(t)$ and $\mu_{I_E}(t)$ represent spatial means for the gap, castellation and interior, respectively. Values for the weight coefficients are listed in Table 1. The time profiles of the spatial statistics for the interior of the electrode are shown in Fig. 3(a). The spatial std statistic is relatively smooth on a frame-by-frame basis whereas the spatial mean statistic exhibits rapid temporal fluctuations.

The spatial mean of the electrode interior, at each time point, is observed to be highly spatially correlated. Near-linear correlation, for example, is shown by the scatter-plot in Fig. 3(b) of the spatial means of Fig. 2 electrode interior sub-regions '1' and '2', $\mu_{I_2}(t)$ versus $\mu_{I_1}(t)$, for the time-course of the DEP experiment ($>10^3$) points. Scatter-plots of other sub-region means, e.g. $\mu_{I_3}(t)$ versus $\mu_{I_1}(t)$, etc., also exhibit high linear correlation (data not shown). This property suggests that a good sample estimate of the dark noise RV can be made using the spatial mean of the intensity of the electrode interior, i.e. $\hat{\mu}_\delta(t) = E[I_\delta(t)] \cong \mu_{I_E}(t)$ where '^' denotes *estimate*. Thus, applying (2), (4), (6), the axiom, $\iota_\varepsilon = 1-\gamma-\chi$, and the above relation, enables an expression for the *modified* spatial mean for the frame (prime denotes modified) to be written as,

$$\mu'_F(t) = \mu_F(t) - \mu_{I_E}(t) = \gamma\,\mu'_G(t) + \chi\,\mu'_C(t) \tag{7}.$$

In (7) the modified spatial means for the gap and castellation regions are also expressed, $\mu'_G(t) = \mu_G(t) - \mu_{I_E}(t)$ and $\mu'_C(t) = \mu_C(t) - \mu_{I_E}(t)$, respectively.

The spatial means and stds for all regions were evaluated according to methods described in the previous section and are shown in Fig. 3(c) to 3(e). Clearly, in all three plots, the std statistic is relatively smooth whereas the mean statistic exhibits rapid temporal fluctuations. A plot of the *modified* frame mean, $\mu'_F(t)$, numerically evaluated using the middle term of (7), is shown in Fig. 3(c); $\mu'_G(t)$ and $\mu'_C(t)$ are plotted for the gap and castellation regions in Fig. 3(d) and 3(e), respectively. The *modified* spatial means for the frame, gap and castellation regions are clearly relatively free of noisy, short-time fluctuations compared with the (unmodified) spatial means, and therefore exhibit higher SNR. Correlation of the frame std with the *modified* spatial mean, shown in Fig. 3(f), is much clearer than for

the scatter-plot for the (unmodified) spatial mean. It exhibits an almost linear relationship for the collection phase and less so for the release phase.

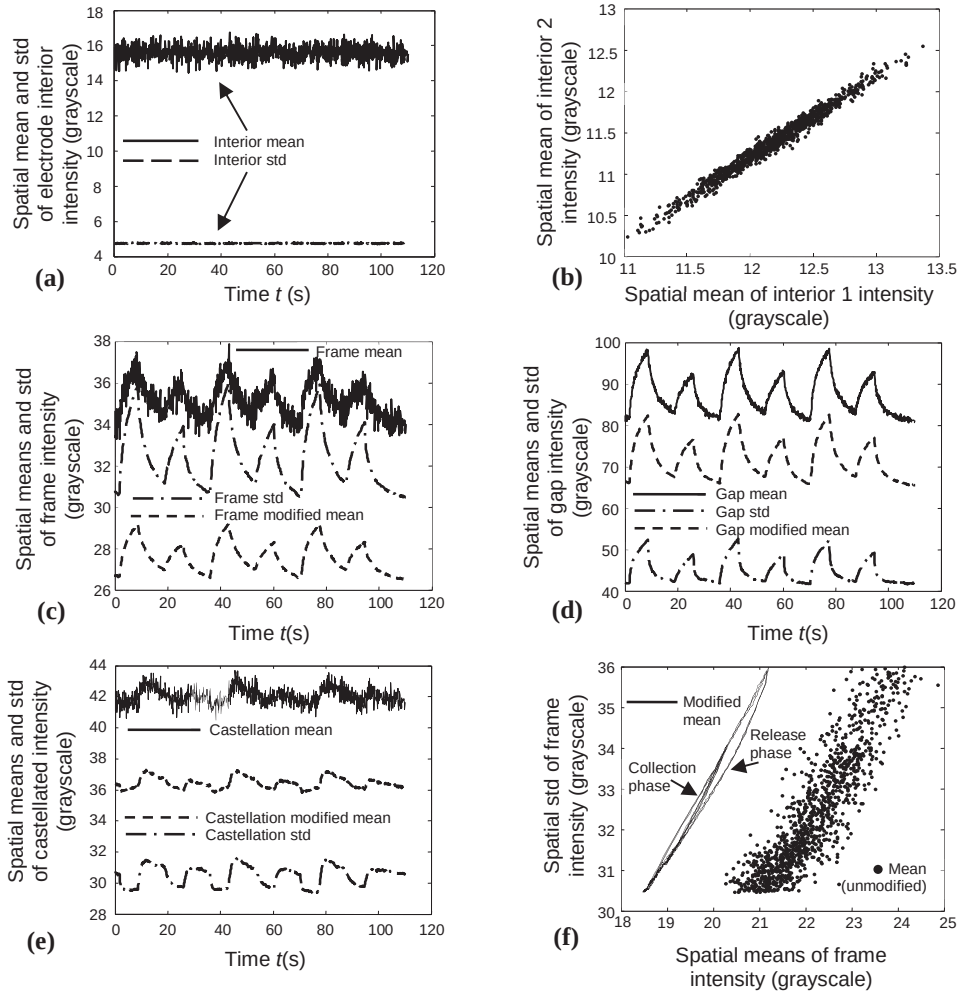


Fig. 3. (a) Intensity of the interior region of the electrode versus time shows that the spatial mean is noisy and the spatial std is relatively smooth. (b) Scatter-plot of spatial means of electrode sub-regional interiors exhibits high correlation. Spatial means and stds for frame, gap and castellation regions, (c) to (e), respectively, versus time. The mean statistics are noisy whereas the *modified* spatial mean has less noise and therefore a higher SNR. (f) Scatter-plot of the spatial std of the frame intensity with the (unmodified) spatial mean for the frame is noisy. In contrast, the spatial std clearly exhibits linear correlation with the *modified* spatial mean during the collection phase. Inconsequentially, for representation only, the modified spatial means in (c) and (e), the spatial std in (d) and unmodified spatial mean in (f), have been shifted 8, 10, 20 and -13 grayscale units, respectively.

## 5. Discussion and concluding remarks

Dual-cycle continuously pulsed pDEP was recently demonstrated as a fast alternative to traditional methods, e.g. cross-over measurements [5, 7], for characterizing nanoparticle surface electrical double-layer conductance[1]. In this work the probe collection frequency has been set at 3.0 MHz for proof-of-concept and the cycles have exhibited very good temporal repeatability. Advancing earlier work [1, 6, 11], we have demonstrated, with experiments supported by a statistical model developed from first principles, a simple and effective way of improving the SNR of the mean, called the *modified* spatial mean statistic. The improved SNR has subsequently revealed a small intensity response of the castellated electrode region, not obvious from single video images, e.g. Fig. 2(e) and (f), that appears out-of-phase with pDEP signaling. It is consistent with nanoparticle depletion, as the castellation bay areas, associated with nDEP, are outside the pDEP capture region. The spatial std of the frame intensity is shown to be almost linearly correlated with the modified mean during the during the collection phase. The collection phase involves mainly deterministic pDEP-driven nanoparticle motion onto a dielectric interface, i.e. metal electrode tips microfabricated on glass. In contrast, the release phase, that involves randomly-driven diffusion away from the electrode tips, results in a spatial std that tends to exhibit a nonlinear 'banana' shaped correlation with the modified spatial mean.

## Acknowledgements

This work was partly funded through a UCL EPSRC Strategic Enterprise Award (GR/T11364/01) awarded to DH. JB was funded through the CoMPLEX Doctoral Training Centre (EP/F500351/1). We thank Professor Gabriel Aeppli and the late Professor Tom Duke for providing laboratory space at LCN, and the cleanroom staff at LCN for technical assistance. DB thanks Professor Hywel Morgan and staff at the University of Southampton for making available electrodes which allowed him to initiate research work at the University of Liverpool. JB thanks Zena Hadjivasiliou for valuable discussions. We thank Dr. Shady Gawad for the loan of the Axiovert 200M microscope.

## References

[1] Bakewell DJ, Bailey J, Holmes D.Real-time dielectrophoretic signaling and image quantification methods for evaluating electrokinetic properties of nanoparticles. *Electrophoresis* 36 (2015) 1443-1450.
[2] Pohl HA. Dielectrophoresis. Cambridge University Press, Cambridge, 1978.
[3] Pethig R. Review Article-Dielectrophoresis: Status of the theory, technology, and applications. *Biomicrofluidics* 4 (2010) 022811: 1-35.
[4] Lapizco-Encinas BH, Rito-Palomares M. Dielectrophoresis for the manipulation of nanobioparticles. *Electrophoresis* 28 (2007) 4521-4538.
[5] Morgan H, Green NG, AC electrokinetics. Research Studies Press, Baldock, England and Institute of Physics Publishing, Philadelphia, USA, 2003.
[6] Gascoyne PRC, Huang Y, Pethig R, Vykoukal J, Becker FF. Dielectrophoretic separation of mammalian cells studied by computerized image analysis. *Meas. Sci. Technol.* 3 (1992) 439-445.
[7] Ermolina I, Milner J, Morgan H. Dielectrophoretic investigation of plant virus particles: Cow Pea Mosaic Virus and Tobacco Mosaic Virus. *Electrophoresis* 27 (2006) 3939-3948.
[8] Henning A, Bier FF, Holzel R, Dielectrophoresis of DNA: Quantification by impedance measurements. *Biomicrofluidics* 4 (2010) 022803: 1-9.
[9] Giraud G, Pethig R, Schulze H, Henihan G, Terry JG, Menachery A, Ciani I, Corrigan D, Campbell CJ, Mount AR, Ghazal P, Walton AJ, Crain J, Bachmann TT. Dielectrophoretic manipulation of ribosomal RNA. *Biomicrofluidics* 5 (2011) 024116: 1-16.
[10] Hawkins BG, Huang C, Arasanipalai S, Kirby BJ. Automated dielectrophoretic characterization of Mycobacterium smegmatis. *Anal. Chem.* 83 (2011) 3507-3515.
[11] Bakewell DJ, Bailey J, Holmes D. Advancing image quantification methods and tools for analysis of nanoparticle electrokinetics. *AIP Advances* 3 (2013) 102101: 1-21.
[12] Dougherty ER. Probability and Statistics for the Engineering, Computing, and Physical Sciences. Prentice-Hall, Englewood Cliffs, 1990.